Published in final edited form as:
Acta Biomater. 2014 July ; 10(7): 2945–2955. doi:10.1016/j.actbio.2014.04.001.

Development of optical probes for *in vivo* imaging of polarized macrophages during foreign body reactions

David W Baker[#a], **Jun Zhou**[#a], **Yi-Ting Tsai**[a], **Kaitlen M Patty**[a], **Hong Weng**[a], **Ewin N. Tang**[a], **Ashwin Nair**[a], **Wen-Jing Hu**[b], and **Liping Tang**[a,c]

[a]Bioengineering Department, The University of Texas at Arlington, Arlington, TX 76019-0138

[b]Progenitec Inc., Arlington, TX 76001-0138

[c]Department of Biomedical Science and Environmental Biology, Kaohsiung Medical University, Kaohsiung 807, Taiwan

[#] These authors contributed equally to this work.

Abstract

Plasticity of macrophages (MΦ) phenotypes exist in a spectrum from classically activated (M1) cells, to alternatively activated (M2) cells, contributing to both the normal healing of tissues and the pathogenesis of implant failure. Here, folate- and mannose-based optical probes were fabricated to simultaneously determine the degree of MΦ polarization. *In vitro* tests show the ability of these probes to specifically target M1 and M2 cells. In an *in vivo* murine model, they were able to distinguish between M1-dominated inflammatory response to infection and M2-dominated regenerative response to particle implants. Finally, the probes were used to assess the inflammatory/ regenerative property of biomaterial implants. Our results show that these probes can be used to monitor and quantify the dynamic processes of MΦ polarization and their role in cellular responses in real time.

Keywords

Macrophage polarization; *In vivo* imaging; Optical probe; Inflammation; Biomaterials

1. Introduction

In the process of wound healing responses, MΦs first become activated to destroy the potential pathogen and subsequently launch regenerative responses to restore tissue homeostasis. Unfortunately, the continuous presence of many medical implants may contribute to a long-term overstimulation of macrophages leading to chronic inflammation

Correspondence to Liping Tang, Ph.D., Department of Bioengineering, University of Texas at Arlington, Box 19138, Arlington, TX 76019-0138, phone: 817-272-6075 fax: 817-272-2251 ltang@uta.edu.

and poor wound healing. This unbalanced reaction, also known as the foreign body response, often leads to implant failure due to the formation of a cellular, protein mediated, capsule which impedes the function of the implant [1-3]. In recent years, increasing knowledge has revealed a link between the contradictory activities and polarization of MΦs [4]. Most commonly, these are grouped into classically activated (M1) cells which are pro-inflammatory in nature, or alternatively activated (M2) cells which are regulatory in nature. These cells exert almost opposite effects on the adaptive immune response triggering either tissue destruction or regeneration [4, 5]. Previous results have shown that MΦ polarization has a profound impact on tumorigenesis, immune responses, and angiogenesis [6-10]. Studies have also confirmed that both classically activated and alternatively activated MΦs can alter tissue response through the degree of activity and cytokine production in models such as pulmonary fibrosis, metastatic disease, and infectious disease [8, 9, 11-13]. There is however, a dearth of information on the relative degree of MΦ polarization that leads to altered destructive/regenerative responses. This scarcity may partially be due to the lack of methods to monitor and quantify the relative polarity of MΦs in real time.

Mounting evidence has supported that, via a plethora of receptors, polarized MΦs are able to respond to different signals in the physiological milieu. In fact, some of these receptors have been used to distinguish between different subsets of polarized MΦs. The folate receptor for instance, has been shown to be up-regulated and specific for macrophages activated by an inflammatory stimulus [14]. The folate receptor, in addition to being expressed in the kidney and placenta, is also up-regulated in many express malignant tissues such as ovarian, breast, bronchial and brain cancers. However, other normal tissues only low or undetectable levels of folate receptor [15, 16]. Thus folate receptors have been the target of several delivery systems for therapeutic drugs, and imaging agents. In a study collecting murine MΦ after peritoneal lavage, it was found that only the activated MΦ subset and not the resident MΦs, granulocytes, lymphocytes, or erythrocytes, expressed up-regulated folate receptors [14]. In addition, these folate receptor positive MΦs also produced reactive oxygen species (ROS) and expressed tumor necrosis factor-α (TNF-α) as well as surface markers for classically activated M1 MΦ . Low levels of surface markers were detected for alternatively activated MΦs [14]. Similarly, the folate receptor has been identified on activated synovial MΦs in rheumatoid arthritis [15] and in MΦs in the pathogenesis of atherosclerosis [16]. We have previously developed a folate receptor-targeting probe to quantify the degree of inflammatory responses around a medical implant. This probe was shown to have high affinity for lipopolysaccharide (LPS) activated MΦs *in vitro* and LPS-induced inflamed tissue *in vivo* [17]. Furthermore the folate receptor-targeting probe was able to detect activated MΦs surrounding biomaterial implants and assess the overall inflammatory reaction to subcutaneous implants [17].

Many recent studies have used the mannose receptor as a target ligand for M2 alternatively activated MΦs. The mannose receptor is an important endocytic receptor which provides a clearance system for molecules up-regulated during inflammation such as tissue plasminogen activator, myeloperoxidase, thyroglobulin, and some microbial ligands [18, 19]. The mannose receptor is expressed by MΦs and select endothelial cells but not by monocytes or neutrophils [19]. Although activated dendritic cells (DCs) have limited

expression of mannose receptor, most of the DCs do not constitutively express mannose receptor *in vivo* [18]. The mannose receptor of MΦs can be substantially up-regulated by stimulation with IL-4, IL-10, and IL-13, although the activation pathways may be different among cytokines [18-20]. Coincidentally, expression of mannose receptor is diminished by interferon- γ (INF-γ) stimulation which is a hallmark initiator of M1 responses [19]. The contrast between the folate receptor and the mannose receptor may therefore provide a vital difference in the detection of polarized macrophages in the context of biomaterial mediated inflammation and resolution. We therefore designed analogous imaging probes coupled with distinct near-infrared (NIR) indicators to simultaneously monitor the dynamic process of macrophage polarization around biomaterial implants.

The following study was aimed at fabricating distinct folate receptor- and mannose receptor-targeting probes which can be used simultaneously to identify and quantify the degree of macrophage polarization *in vivo*. Specifically, folate- and mannose- conjugated NIR probes were fabricated by covalently linking ligands with NIR dye-labeling polyethylene glycol (PEG) platform. For simultaneous imaging, folate was linked to Oyster800 dye (Emission: 796 nm) and mannose linked to Oyster680 dye (Emission: 693 nm). The toxicity and efficiency of the imaging probes to recognize activated M1 or M2 cells was then assessed *in vitro*. Their applicability for *in vivo* imaging was then investigated using BALB/c mice and subcutaneous implantation of poly(lactic acid) (PLA) particles. In a model of infection, some of these particles were mixed with either LPS or *Staphylococcus aureus* bacteria to investigate the ability of the probes to monitor infection-related complications and the resolution of such responses. By comparing NIR probe fluorescence intensities and histological evaluation, we explored the possibility of using folate- and mannose-based probes to monitor and quantify the extent of such reactions. Finally, using a well-established particle implant model, we determined the ability of the probes to assess the resolution of inflammatory response to various biomaterials by imaging M1 and M2 *in vivo*. The ability to simultaneously monitor both M1 and M2 responses and the dynamic effects of these cells in real time may greatly improve our understanding and lead to enhanced methods to evaluate and diagnose implant safety and performance.

2. Materials and methods

2.1. Materials

Both linear NH_2-PEG-COOH (Mw:5k) and linear *t*-BOC-PEG-NH_2 (Mw:5k) were purchased from JenKem Technology USA Inc (Allen, TX). Oyster®-800 TFP ester (Oyster800) and Oyster®-680 TFP ester (Oyster680) were purchased from Boca Scientific Inc (Boca Raton, FL). Folic acid, 4-aminophenyl α-D-mannopyranoside (Mannose), N-hydroxysuccinimide (NHS), *N*,*N*′-Dicyclohexylcarbodiimide (DCC), 1-Ethyl-3-(3-(dimethlaminopropyl) carbodiimide (EDC), and all other chemicals were purchased from Sigma-Aldrich (St Louis, MO).

2.2. Preparation of folate- and mannose-based probes

Both folate- and mannose-based probes were fabricated using PEG linear polymer as a carrier with one ligand and one fluorophore per probe. The folate-based probe was prepared

as described in a previous publication with minor modification [21]. Briefly, folic acid (FA, 50 mM) was dissolved in dimethyl sulfoxide (DMSO), and then DCC (100 mM) and NHS (100 mM) were added to the above folic acid solution. The mixture was incubated overnight at room temperature, and then the byproduct 1,3-dicyclohexylurea was removed by centrifuge. The above-prepared activated folic acid (80 mM) solution was mixed with *t*-BOC-PEG-NH_2 (4.0 mM) and the mixture was incubated for 24hrs at room temperature to couple folic acid to amine group of *t*-BOC-PEG-NH_2 (*t*-BOCPEG-FA). The intermediate was dialyzed exhaustedly against DMSO and then against DI water (Spectra/Por® 1-7 Regenerated Cellulose Membrane, cutoff:3.5K, Spectrum Laboratories Inc.). The dried intermediates were dissolved in dichloromethane and then treated with trifluoroacetic acid to cleave *t*-BOC groups (NH_2-PEG-FA). After purifying against DI water and lyophilizing, the folate-based probe was prepared by incubating Oyster800 TFP ester and NH_2-PEG-FA (molar ratio:1.5/1) in PBS buffering solution (pH:8.2) for 24 hrs at room temperature. The unconjugated dye was removed by dialysis against DI water until undetectable by UV-visible spectrometer and/or fluorometer. The obtained probe was freeze-dried and stored at 4°C for further use.

For preparation of the mannose-based probe, a similar method was carried out using an established EDC procedure [22, 23]. Briefly, Oyster680 TFP ester and NH_2-PEG-COOH (molar ratio: 1.5/1) were incubated in PBS buffering solution (pH 8.2) for 24 hrs at room temperature to obtain Oyster680-PEG-COOH. The Oyster680-PEG-COOH was dialyzed against DI water until no free dye was detectable in dialysate solution using UV-visible spectrometer and/or fluorometer. After freeze drying, EDC was added to 4-aminophenyl α-D-mannopyranoside and Oyster680-PEG-COOH PBS buffering solution (pH 4.8) (molar ratio: Oyster680-PEG-COOH:EDC:4-aminophenyl α-D-mannopyranoside = 1:35:30). The mixture solution was incubated 24 hrs at room temperature to obtain the mannose-based probe. The probe was purified thorough dialysis and freeze dried for further use. Chemical structures of both folate- and mannose-based probes were characterized using Nicolet 6700 FT-IR Spectrometer (Thermo Nicolet Corp., Madison, WI). Optical properties of two probes were analyzed using a microplate reader (Infinite® M200; Tecan Group Ltd, Mannedorf, Switzerland). To normalize fluorescence intensity from the plate reader the highest peak intensity was taken to be “100”. Based on NMR measurements, the folate/PEG and mannose/PEG conjugation efficiencies was >90% which concurs with previous work [24].

2.3. Cell isolation and culture procedures

Primary murine MΦs were obtained as previously described [25, 26]. Briefly, the bone marrow from the femur and tibia of 6-8wk old BALB/c mice was flushed with Dulbeco’s modified eagle medium (DMEM) (Sigma) with 20% fetal bovine serum (FBS) (Atlanta Biologicals). Cells were then plated into 25cm^2 tissue culture flasks with a bone marrow macrophage media (BMMO) (10% FBS, 10% L929 fibroblast conditioned medium, 1% HEPES, 1% non-essential amino acids (Life Tech, Grand Island, NY.), 1% sodium pyruvate, and 1% penicillin-streptomycin (AB) in Dulbecco’s modified Eagle’s medium) [26]. MΦ were allowed to mature for 10 days before further subculture and separation into well plates at specified densities from 2000 to 50,000 cells/well. 3T3 Swiss albino fibroblasts were obtained from American Tissue Culture Collection (ATCC, Manassas, VA.)

and cultured in DMEM with 10%FBS and 1% AB. All cells were cultured at an ambient temperature of 37°C in a 5% CO_2 incubator.

2.4. M1/M2 differentiation

After 10 days in culture, some MΦs were differentiated to classically activated $_{M1}$ cells by the addition of LPS (from E-coli, Sigma St. Louis MO) (1μg/ml) for 24 hours according to previous publication [27]. Other cells were differentiated to alternatively activated M2 cells by the addition of IL-4 and IL-13 to BMMO media (10ng/ml IL-4 and 10ng/ml IL-13 for 24 hours) as previously described [28, 29]. After 24 hours of differentiation, cell subsets (M1 lineage- $CD80^+$, M2 lineage – $CD206^+$) were confirmed morphologically and through immunohistochemical staining methods as previously documented [30, 31].

2.5. *In vitro* probe analysis

Differentiated cells were used to assess the specificity and efficacy of the imaging probes to monitor M1/M2 cell density *in vitro*. For this, both imaging probes (25 μg/ml) were added and then incubated with cells for 30 minutes (established in preliminary studies) in a competition binding test. The cells were then washed thrice with hanks buffered salt solution. The fluorescence intensities were then read on a Tecan Infinite MΦ 200 plate reader (San Jose, CA) at excitation 730 emission 800, and excitation 630 emission 700 for the folate- and mannose-based probes respectively. Background intensity, determined from wells containing media without any cells, was subtracted to obtain final fluorescence intensities. Cytotoxicity studies were performed with 3T3 Swiss albino fibroblasts as described earlier [17]. Briefly, 5,000 cells were plated into wells of a 96 well plate, cells were allowed to adhere overnight before the addition of folate- or mannose-based probes at specified concentrations from 0 to 62.5 μg/ml. After 24 hours incubation period MTS assay (CellTiter96®, Promega, USA) was run on the cell samples, according with the manufactures instructions, and percent cell survival was compared to 0% probe as controls. Measurement of absorbance was performed on a SpectraMax 340 spectrophotometer (Molecular Devices, USA).

2.6. Polymeric particles used as model biomaterial implants

Both infection and particle implant-associated inflammation models were used in this investigation. All mice used in this study were female BALB/c mice purchased from Taconic Farms (German town NY). All animal experiments were approved by the University of Texas at Arlington Animal Care and Use Committee (IACUC) and in accordance with the National Institutes of Health guidelines for the use of laboratory animals. Poly (N- isopropylacrylamide) (PNIPAM, D: 100 nm) and poly-lactic acid (PLA, D: 5-10 μm) were used as model biomaterial implants [17, 32]. To mimic implant-associated infection, LPS (5% solution in saline) was mixed with PLA particles to yield a final concentration of 10% PLA and 0.2% LPS. The LPS+PLA particles (100 μl/implant site) were then administered into the subcutaneous space on the back of the animals as described earlier [21]. To simulate bacterial infection, 10% PLA w/v was mixed into a 100 μl saline solution containing 1.6×10^8 cfu *Staphylococcus aureus* - Xen29 bacteria (Caliper LifeSciences, Alameda, CA) prior to subcutaneous transplantation. One day after

implantation, the probes were administered by retro-orbital injection (total volume 100 μl contains 10 μl folate-based probe (1.0 mg/ml, equivalent to 0.14 mM dye concentration) +10 μl mannose-based probe (1.0 mg/ml, equivalent to 0.14 mM dye concentration) + 80 μl saline). To model biomaterial implants, PLA and PNIPAM particles (100 μl, 10% w/v in saline) were subcutaneously implanted on either side of the dorsal region in mice via a 25 gauge needle. Using doses as injected in the above infection model, the probes were administered via retro-orbital injection 1, 4, 7 and 14 days after implantation.

2.7. *In vivo* imaging

Two days after probe injection, whole body fluorescence images are taken using the Kodak in-vivo FX Pro system (f-stop:2.5, 4x4 binning: Carestream Health, Rochester, NY). To simultaneously monitor the folate- and mannose-based probes an excitation filter 760 nm: emission 830 nm, and an excitation filter 630 nm: emission 700 nm are used respectively. To co-register the fluorescence signals from both mannose-based probes and folate-based probes with minimal cross-excitation, we chose to use lower excitation wavelength (630 nm) for mannose-based probes instead of the regular excitation wavelength (680 nm). For fluorescent intensity calculation, a region of interest (ROI) (area in pixels) was first drawn over the induced fluorescent signal using Carestream Molecular imaging software (ROI-1). The software then calculated the mean intensity for all pixels within ROI-1. A second ROI was then drawn over a control or “background” area (area with no induced fluorescence) (ROI-2). Again, the mean intensity for all pixels within ROI-2 was calculated by the software. To normalize the intensity data, background correction was performed, that is, the mean intensity for ROI-2 was subtracted from the mean intensity of ROI-1. This calculation gives the fluorescence intensity value of the induced fluorescence from the imaging probe. For bio-distribution study, all organs and implant site tissue were isolated from animals after probe administration for 24 hours. The organs/tissues were then imaged using a Kodak *in vivo* imaging system to quantify the organ fluorescence intensities. All data analyses are performed with the Carestream Molecular Imaging software, network edition 4.5 (Carestream Health, Woodbridge, CT.)

2.8. Immunohistochemical and histological analysis

After the final imaging analysis, animals were euthanized and implants and surrounding tissues were isolated for further analysis. Tissues were embedded into OCT and 7 μm thick cross sections were cut. Hematoxylin and Eosin staining (H&E staining) (Sigma) was used to determine the extent of inflammatory response to the implants. Collagen density was determined via Masson’s trichrome stain. The capsule thickness was determined as described previously by measuring the distance from the biomaterial perpendicular toward the native healthy tissue of the hypodermis using NIH ImageJ software [33]. The degree of MΦ polarization (M1 $CD80^+$ cells and M2 $CD206^+$ cells) and inflammatory responses (CD11b+ cells) was assessed through immunohistochemistry. All antibodies used were purchased from Santa Cruz Biotech (Santa Cruz, CA). Secondary antibodies were purchased from ProSci (Poway, CA), and nuclei were stained with DAPI (Invitrogen, Carlsbad, CA). Cell densities were calculated as the number of positive cells per field of view using similar areas for all counts. All histological and immunohistochemical analysis was performed on a Leica microscope (Leica, Wetzlar Germany) and processed using NIH ImageJ software.

2.9. Statistics

GraphPad (La Jolla, CA) was used for all statistical operations. Results are reported as the means ± standard deviations. Differences between treatment groups were assessed using ANOVA with Bonferroni correction for data with multiple group comparisons. The student's t-test was performed for data with single group comparisons. In each *in vivo* experiment a total of six mice (6-8 wk old female BALB/c mice) were used, unless otherwise specified. All data were considered significant when $P<0.05$(*) or $P < 0.01$(**). Linear regression analyses were also used to determine the correlation between group comparisons by calculating the coefficient of determination (R^2).

3. Results

3.1. Fabrication and characterization of folate- and mannose-based probes

To fabricate the probes, PEG particles were used as the carrier of the ligands and dyes. The probes were fabricated first by conjugation of NIR dyes with NH_2-PEG-COOH polymer. The dye-conjugated polymers were then covalently linked to either folate or mannose molecules via carbodiimide coupling chemistry. Using Fourier transform infrared analysis (FTIR), we confirmed the conjugation of folate and mannose moieties into PEG (Figure 1A, C). The FTIR spectra of PEG, folate-based probe and folate are shown in Figure 1A. The FTIR spectrum of the folate-based probe displays characteristic peaks at 1680 cm^{-1}, due to the amide link between PEG and folic acid, as well as 1600 and 1410 cm^{-1} which can be attributed to the benzene ring of folate [34, 35]. The FTIR spectra of PEG, mannose-based probe and mannose are shown in Figure 1C. Characteristic IR absorption peaks are observed for PEG at 1100 and 1345 cm^{-1} corresponding to the C-O-C stretching, and at 950 cm^{-1} for C-H bending [35]. The FTIR spectrum of the mannose-based probe shows a C=N stretch at 1660cm^{-1} demonstrating the conjugation of mannose to PEG as well as the presence of the amide bond at 1390 cm^{-1} [36].

To simultaneously monitor both M1 and M2 responses, it is important that both probes can be imaged independently *in vivo* without interference. To accomplish this Oyster800 and Oyster680 dyes were chosen with characteristic excitation and emission bands having little to no overlap with emission signals. This was confirmed by mixing the probes in an aqueous solution (PBS) and monitoring the excitation and emission spectra (Figure 1B, D). As expected the two probes show individual excitation emission spectra with maximal emission of the folate-based probe at 800 nm and maximal emission of the mannose-based probe at 700 nm wavelength.

3.2. Effectiveness of folate- and mannose-based probes on targeting M1 and M2 cells *in vitro*

We further carried out *in vitro* studies to demonstrate the effectiveness of the probes in targeting M1 and M2 cells. After 24 hours of differentiation, cell lineage was confirmed through morphological and immunohistochemical analysis. As expected, most cells showed spindle morphology with a high degree of spreading and also stained positive for the activation marker CD80 (Figure 2A) which are typical phenotypes of inflammatory activated MΦ [14]. In contrast, the MΦ cells cultured with IL-4 and IL-13 showed a broader

round morphology and stained positive for CD206 (Figure 2A), a known M2 differentiation marker [31]. The cytotoxicity of folate- and mannose-based probes was further determined using 3T3 fibroblasts and a standard MTS assay (Figure 2B). We found that both probes were well tolerated in 3T3 cells over the studied concentration range (up to 62.5 μg/ml) with no statistical differences from the control.

To investigate the probes' specificity to target either M1 or M2 with minimal cross probe interference, we performed a competition binding test. Our hypothesis was that in a mixed probe solution, only the folate-based probes would bind to a population of entirely M1 cells, and only the mannose-based probes would bind to a population of entirely M2 cells, within a shortened time span of 30 minutes. As expected, incubation of probes with either M1 or M2 MΦ cells showed good cellular specificity (Figure 2 C, D). Over the various densities tested the folate-based probe was found to bind primarily to M1 cells (Figure 2C) and the mannose-based probe was found to bind primarily to M2 cells (Figure 2D). We also found that fluorophores themselves (control probes) have no or little affinity to cells (Figure 2E-F). In both cases, the difference was enhanced by an increasing cell number in a near linear fashion, while the intensity of the opposing probe remained almost constant, indicating minimal to no binding and minimal phagocytosis within the short time frame. In figure 2 C and D, linear trend lines are shown for the folate-based probe and M1 cells (correlation coefficient R^2=0.914) and the mannose-based probe and M2 cells (R^2=0.94), respectively. It should be noted when the cell numbers below 15,000, there was no linear relationship between fluorescent intensities and cell numbers. Overall, these results support our hypothesis that the folate receptor and mannose receptor may be used as target ligands to distinguish between M1 and M2 cell populations *in vitro*.

Further study was carried out to investigate the bio-distribution of both probes in mice after administration for 24 hours (Figure 3A-B). We observed the difference in bio-distribution for the two probes. For folate-based probe, large quantities of the probe were found in the kidney while some accumulated in the liver, spleen and stomach. On the other hand, for mannose-based probe, most probes accumulated in the stomach, while small quantities of probes were found in the lung, liver and kidney. These results show that, despite of similar physical structure, these two probes have drastically different biological affinities.

3.3. Monitoring and quantifying MΦ responses in an infection model

It is well established that M1 MΦ responses are critical to infection-mediated immunity and device-centered infection [37-39]. We thus tested the possibility of using folate- and mannose-based probes to distinguish between infected and bacteria-free implants. To simulate infected implants, some of the PLA particles were incubated with either lipopolysaccharide (LPS) or live bacteria prior to implantation. As expected, we found a substantial increase in the accumulation of folate-based probes at the sites of LPS and bacteria in comparison to the PLA controls (Figure 4A). On the other hand, we observed significantly less mannose-based probe accumulation at the LPS and bacteria implant sites in comparison to controls (Figure 4A). Immunohistochemical analysis (Figure S1) demonstrated that PLA alone showed a low M1 response with a respective high M2 response. In contrast, PLA+Bacteria showed a high M1 response with a respective low M2

response. Comparison to histological and immunohistochemical analysis confirmed a linear relationship either between M1 (CD80) cell density and fluorescence intensity of folate-based probe (R^2= 0.973) (Figure 4B) or between M2 (CD206) cell density and fluorescence intensity mannose-based probe (R^2= 0.954) (Figure 4C). Furthermore, the M2/M1 ratios for both the intensities from *in vivo* imaging and the cell numbers from immunohistochemical staining were substantially lower at the implant sites for LPS and bacteria than for the controls (Figure 4D). These results suggest that the presence of LPS or bacteria would substantially increase M1 differentiation while diminishing M2 differentiation. As a result, infected implants are likely to promote chronic inflammation. In confirmation of this, as expected, we observed that both LPS and bacteria-embedded implants had a substantially increased capsule thickness at 133 ±13 μm and 132±27 μm respectively in comparison to the control PLA implants with a tissue capsule thickness of only 91 ±9.8 μm. At last, we correlated the fluorescence intensity ratio of mannose-based probe to folate-based probe with the cell ratio of CD206 cells to CD80 cells, and found the existence of a strong relationship (R^2= 0.9857) (Figure 4E). Taken together, our data indicates that by determining fluorescence intensity ratio of the folate-based probes to mannose-based probes, we are able to assess the relative degree of M1 and M2 cells across two distinct infection models.

3.4. Monitoring and quantifying biomaterial-associated tissue reactions with folate- and mannose-based probes

Next, to determine whether fluorescence intensity ratio of M2/M1 can be used to assess biomaterial-associated inflammatory and regenerative responses *in vivo*, we used PLA and PNIPAM microparticles as model implants. Both PLA and PNIPAM are commonly employed in several studies for both drug delivery and tissue engineering. Although extensively used, PLA microparticles are known to elicit an inflammatory response resulting in the formation of a fibrotic capsule [40]. PNIPAM on the other hand is much more biocompatible and does not lead to a chronic inflammatory response [41]. We thus employed PNIPAM and PLA particles as model materials with distinct tissue reactivity. After subcutaneous implantation for 1, 4, 7 and 14 days, folate- and mannose-based probes were administered *i.v.* and whole body images were then taken after an additional 48 hours. Interestingly, at day 1, there were no significant differences between the fluorescence intensities ratio of M2/M1 at the PLA and PNIPAM sites (Figure 5A). However, at days 4, 7 and 14, the fluorescence intensity ratios of M2/M1 around PLA implants were significantly reduced while the M2/M1 ratios at PNIPAM sites remain high are significantly higher than those at the PLA sites (Figure 5A). The *in vivo* imaging data suggests that statistically higher M2/M1 ratios associated with the PNIPAM implants may lead to reduced inflammatory reactions and increased regenerative responses. To test this hypothesis, we performed histological analysis to quantify inflammatory cell number, capsule thickness and collagen density in 14-day implants. The relationship between M2/M1 ratios and histological evaluations was then determined. As expected, we first found that the PLA implants triggered the accumulation of more CD11b+ inflammatory cells than PNIPAM implants (49/field of vision vs 20/field of vision). On the other hand, M2/M1 ratios are significantly higher on PNIPAM implants than on PLA (Figure 5B). To validate the distribution of the folate- and mannose-based probes within the implantation sites, tissue sections bearing PLA

implants were observed under a fluorescence microscope (Figure S2). It was found that a high concentration of mannose-based probes (green color) was present in tissue neighbouring PLA implants, while lower amounts of folate-based probes (red color) were detected surrounding the PLA implants. Subsequent histological studies revealed that the PLA implants prompt 2.4 times higher capsule thickness compared to PNIPAM implants (109.1±8.5 μm vs. 45.4±9.3 μm). Interestingly, we found an inverse and statistically significant relationship between M2/M1 ratios and capsule thickness (R^2= 0.90, Figure 5C). Finally, capsule collagen densities were determined to reflect the extent of implant-associated fibrotic tissue responses. For that, we found that the PLA implants generate 2.0 times higher collagen density than the PNIPAM implants (42.9±4.3% vs. 21.8±2.1%). Similar to capsule thickness, we found an inverse relationship between capsule collagen densities and M2/M1 ratios (R^2=0.86, Figure 5D). Taken together, we found that the folate- and mannose-based probes are able to differentially monitor the dynamic changes in the M1 and M2 response around biomaterial implants with various inflammatory characteristics, and more importantly we were able to assess the extent of inflammatory/regenerative responses *in vivo*.

4. Discussion

Imaging modalities to monitor *in vivo* inflammatory responses are becoming increasingly important to both basic research and clinical applications. Many newly developed techniques provide fast, accurate, and minimally invasive assessment of the overall extent of inflammatory cell responses. Substantial research efforts have been placed on investigating the influence of polarized MΦs, M1 vs. M2 cells, to determine the balance between immune rejection and tissue regeneration [30, 31]. It was found that higher ratios of M2/M1 MΦ were associated with more positive remodeling outcomes, and that the constructive remodeling outcome may be due to the recruitment of different cell populations with materials that elicit an M1 or an M2 response [31]. While many studies have assessed the dynamics of MΦ polarization *in vitro*, few studies have shown the dynamic polarized MΦ responses *in vivo*. Here we have developed an imaging probe system to non-invasively and simultaneously evaluate the balanced interactions between polarized inflammatory M1 and regenerative M2 MΦs.

The up-regulation of both the folate receptor and the mannose receptor on activated MΦs has been studied extensively as targets for both imaging modalities and drug delivery vehicles. The folate receptor has been shown to be expressed on activated synovial MΦs from rheumatoid arthritis as well as several malignant cancers and as such has been investigated in several arthritic and cancer models [15, 42-44]. In addition, as previously mentioned, binding ability of folate to murine peritoneal MΦs is only detected after an inflammatory stimulus [14]. On the other hand, targeting of mannose receptor has been exploited for delivering drugs to MΦs either by direct conjugation [45], through mannose coated liposomes [46, 47], or through polymer microspheres [36, 48]. While the use of mannose as an alternative activation marker is relatively undisputed, some evidence indicates that the folate receptor β can also be used to mark M2 regulatory cells [49]. Here, we aim to determine the relative degree of inflammatory vs. regulatory MΦs. Our studies

indicate that the folate- and mannose-based probes can accurately determine real-time recruitment and differentiation of the inflammatory and regulatory subsets of MΦs.

Our *in vitro* studies demonstrate that the developed M1 and M2 probes have minimal cytotoxicity and are able to distinctly monitor activated M1 and M2 cells *in vitro*. For these studies, MΦs were cultured from the bone marrow of BALB/c mice and differentiated to either M1 by LPS or M2 by the addition of IL-4 and IL-13. Previous results have shown that MΦ polarization may be controlled *in vitro* by stimulation with IFN- or LPS (M1) or IL-4 & IL-13 (M2) [5, 19]. Additionally, a further subset of alternatively activated MΦ may be produced by stimulation with IL-10 (M2) [5]. LPS is well known to activate MΦ through the TLR4 receptor resulting in cytokine production of M1 pro-inflammatory mediators such as IFN-, IL-2 and TNF-α [50]. Similarly, several recent studies have shown that MΦ cell lines such as RAW264.7 or U937 monocytes may be induced to express high levels of folic acid receptors by LPS stimulation [16, 51]. Our *in vitro* studies indicate that folate receptor was induced on bone marrow MΦs from BALB/c mice by the increasing intensity of the folate-based probe but not the mannose-based probe in LPS activated M. In the competition binding study, had folate receptor not been induced, it would be expected that the level of the folate-based probe and mannose-based probe would be similar due to nonspecific binding or phagocytosis, as it is, this was not the case and only uptake of folate-based probe was increased with increasing cell concentration. Similarly, the competition binding studies show that only the mannose-based probe had enhanced uptake with increasing numbers of M2 cells, but not M1 cells. Furthermore, it should be noted that, for the folate probe, competitive binding assay study was reported in one of our recent publications.[17] A similar study has also been carried out on the mannose probe by another group.[52]

Device-centered infection is one of the common causes of implant failure due to chronic inflammatory responses [53, 54]. In fact, *Staphylococcus aureus* can be recovered from approximately 90% of clean wounds at the time of closure [53]. This indicates that even when all appropriate steps are taken, the possibility of infection remains high and should be regarded with concern. It is well established that LPS prompts a localized inflammatory response with the increased accumulation of inflammatory cells and mediators including activated MΦ [55-57]. Similarly, pathogens, including *Staphylococcus aureus* bacteria, are known to induce a range of activation profiles for MΦ priming the cells to mount an immune response [58]. Since the majority of MΦs at the site of the infection are M1 cells, we further investigated whether the folate- and mannose-based probes can be used for real time detection of infection. As expected, we observed that higher numbers of M1 MΦs were recruited to particle implants infected by either LPS of live bacteria. In addition, we found a good relationship between M2/M1 ratios and fibrotic tissue reactions. In a direct correlation, the folate- and mannose-based probes were able to accurately show the relative cellular density for the M1 and M2 cells for each of these model implants in the infection model.

To further explore the effectiveness of the folate- and mannose-based probes *in vivo* we employed polymer particles as model biomaterial implants. Our results show that discernible differences can be observed with *in vivo* imaging of the MΦ response to PLA and PNIPAM particle implants. We chose PLA and PNIPAM particles, since both are commonly used for fabricating tissue engineering scaffolds, drug delivery, and imaging particles [41, 56, 59,

60]. In addition, PLA particles represent typical strong foreign body reactions while minimal inflammatory responses were induced by PNIPAM implants as established in our earlier studies [61]. As anticipated, we were able to observe the higher fluorescence intensity ratio of mannose-based (M2) probe to folate-based (M1) probe at the PNIPAM particle implant sites than at the PLA sites. These results are further confirmed through histological analysis (inflammatory cell, capsule thickness and collagen density) showing almost identical trends to that observed with *in vivo* imaging of M2/M1 ratios with inverse and near linear correlations. These results present a positive example to assess the extent of inflammatory cellular responses by monitoring M2/M1 cell ratios via *in vivo* imaging in real time.

5. Conclusion

Polarized MΦs (M1 and M2 cells) have been shown to play an important role in controlling the balance between inflammatory and fibrotic responses. Despite intense research efforts, the influence of polarized MΦs compositions at the inflamed tissue sites on the subsequence tissue responses has not been systematically studied due to, at least partially, the lack of a method to monitor MΦ polarization in real time. To overcome this limitation and as the result of this work, folate- and mannose-conjugated polyethylene glycol polymer-based optical probes were fabricated to target M1 and M2 cells, respectively. Our results show that the twin probes were able to provide heightened sensitivity and reliability in the assessment of cellular responses to biomaterials and to enhance our understanding of the dynamic processes of MΦ polarization. We believe that improved knowledge obtained from this new probe system would assist the future development of new biomaterials and strategies to elicit a preferential MΦ response to favor tissue regeneration.

Supplementary Material

Refer to Web version on PubMed Central for supplementary material.

Acknowledgments

We thank National Institutes of Health (NIH) for the financial support (NIH Grants EB014404 and GM101776). In addition, we would like to thank Dr. Baohong Yuan and Ms. Yuan Liu for their help on preparing the near-infrared images (supplementary Figure 2).

References

[1]. Tang L, Eaton JW. Natural responses to unnatural materials: A molecular mechanism for foreign body reactions. Mol Med. 1999; 5:351–8. [PubMed: 10415159]

[2]. Thomsen P, Gretzer C. Macrophage interactions with modified material surfaces. Curr Opin Solid St M. 2001; 5:163–76.

[3]. Tang L, Eaton JW. Inflammatory responses to biomaterials. Am J Clin Pathol. 1995; 103:466–71. [PubMed: 7726145]

[4]. Stout RD, Suttles J. Functional plasticity of macrophages: reversible adaptation to changing microenvironments. J Leukoc Biol. 2004; 76:509–13. [PubMed: 15218057]

[5]. Martinez FO, Sica A, Mantovani A, Locati M. Macrophage activation and polarization. Front Biosci. 2008; 13:453–61. [PubMed: 17981560]

[6]. Kodelja V, Muller C, Tenorio S, Schebesch C, Orfanos CE, Goerdt S. Differences in angiogenic potential of classically vs alternatively activated macrophages. Immunobiology. 1997; 197:478–93. [PubMed: 9413747]

[7]. Sinha P, Clements VK, Ostrand-Rosenberg S. Reduction of myeloid-derived suppressor cells and induction of M1 macrophages facilitate the rejection of established metastatic disease. J Immunol. 2005; 174:636–45. [PubMed: 15634881]

[8]. Arora S, Hernandez Y, Erb-Downward JR, McDonald RA, Toews GB, Huffnagle GB. Role of IFN-gamma in regulating T2 immunity and the development of alternatively activated macrophages during allergic bronchopulmonary mycosis. J Immunol. 2005; 174:6346–56. [PubMed: 15879135]

[9]. Arora S, Olszewski MA, Tsang TM, McDonald RA, Toews GB, Huffnagle GB. Effect of cytokine interplay on macrophage polarization during chronic pulmonary infection with Cryptococcus neoformans. Infect Immun. 2011; 79:1915–26. [PubMed: 21383052]

[10]. Buhtoiarov IN, Lum H, Berke G, Paulnock DM, Sondel PM, Rakhmilevich AL. CD40 ligation activates murine macrophages via an IFN-gamma-dependent mechanism resulting in tumor cell destruction in vitro. J Immunol. 2005; 174:6013–22. [PubMed: 15879094]

[11]. Gratchev A, Kzhyshkowska J, Kothe K, Muller-Molinet I, Kannookadan S, Utikal J, et al. Mphi1 and Mphi2 can be re-polarized by Th2 or Th1 cytokines, respectively, and respond to exogenous danger signals. Immunobiology. 2006; 211:473–86. [PubMed: 16920487]

[12]. Sun L, Louie MC, Vannella KM, Wilke CA, LeVine AM, Moore BB, et al. New concepts of IL-10-induced lung fibrosis: fibrocyte recruitment and M2 activation in a CCL2/CCR2 axis. Am J Physiol Lung Cell Mol Physiol. 2011; 300:L341–53. [PubMed: 21131395]

[13]. Gordon S, Martinez FO. Alternative activation of macrophages: mechanism and functions. Immunity. 2010; 32:593–604. [PubMed: 20510870]

[14]. Xia W, Hilgenbrink AR, Matteson EL, Lockwood MB, Cheng JX, Low PS. A functional folate receptor is induced during macrophage activation and can be used to target drugs to activated macrophages. Blood. 2009; 113:438–46. [PubMed: 18952896]

[15]. Turk MJ, Breur GJ, Widmer WR, Paulos CM, Xu LC, Grote LA, et al. Folate-targeted imaging of activated macrophages in rats with adjuvant-induced arthritis. Arthritis Rheum. 2002; 46:1947–55. [PubMed: 12124880]

[16]. Antohe F, Radulescu L, Puchianu E, Kennedy MD, Low PS, Simionescu M. Increased uptake of folate conjugates by activated macrophages in experimental hyperlipemia. Cell Tissue Res. 2005; 320:277–85. [PubMed: 15714274]

[17]. Zhou J, Tsai YT, Weng H, Baker DW, Tang L. Real time monitoring of biomaterial-mediated inflammatory responses via macrophage-targeting NIR nanoprobes. Biomaterials. 2011; 32:9383–90. [PubMed: 21893338]

[18]. Martinez-Pomares L, Reid DM, Brown GD, Taylor PR, Stillion RJ, Linehan SA, et al. Analysis of mannose receptor regulation by IL-4, IL-10, and proteolytic processing using novel monoclonal antibodies. J Leukoc Biol. 2003; 73:604–13. [PubMed: 12714575]

[19]. Gordon S. Alternative activation of macrophages. Nat Rev Immunol. 2003; 3:23–35. [PubMed: 12511873]

[20]. Stein M, Keshav S, Harris N, Gordon S. Interleukin 4 potently enhances murine macrophage mannose receptor activity: a marker of alternative immunologic macrophage activation. J Exp Med. 1992; 176:287–92. [PubMed: 1613462]

[21]. Zhou J, Tsai YT, Weng H, Tang EN, Nair A, Dave DP, et al. Real-time detection of implant-associated neutrophil responses using a formyl peptide receptor-targeting NIR nanoprobe. Int J Nanomedicine. 2012; 7:2057–68. [PubMed: 22619542]

[22]. Dube D, Francis M, Leroux JC, Winnik FM. Preparation and tumor cell uptake of poly(N-isopropylacrylamide) folate conjugates. Bioconjug Chem. 2002; 13:685–92. [PubMed: 12009963]

[23]. Nayak S, Lee H, Chmielewski J, Lyon LA. Folate-mediated cell targeting and cytotoxicity using thermoresponsive microgels. J Am Chem Soc. 2004; 126:10258–9. [PubMed: 15315434]

[24]. Liu F, Deng D, Chen X, Qian Z, Achilefu S, Gu Y. Folate-polyethylene glycol conjugated near-infrared fluorescence probe with high targeting affinity and sensitivity for in vivo early tumor diagnosis. Mol Imaging Biol. 2010; 12:595–607. [PubMed: 20376571]

[25]. Suzuki K, Kiyokawa N, Taguchi T, Takenouchi H, Saito M, Shimizu T, et al. Characterization of monocyte-macrophage-lineage cells induced from CD34+ bone marrow cells in vitro. Int J Hematol. 2007; 85:384–9. [PubMed: 17562612]

[26]. Godek ML, Sampson JA, Duchsherer NL, McElwee Q, Grainger DW. Rho GTPase protein expression and activation in murine monocytes/macrophages is not modulated by model biomaterial surfaces in serum-containing in vitro cultures. J Biomater Sci Polym Ed. 2006; 17:1141–58. [PubMed: 17235380]

[27]. Paul NE, Skazik C, Harwardt M, Bartneck M, Denecke B, Klee D, et al. Topographical control of human macrophages by a regularly microstructured polyvinylidene fluoride surface. Biomaterials. 2008; 29:4056–64. [PubMed: 18667233]

[28]. Hesse M, Modolell M, La Flamme AC, Schito M, Fuentes JM, Cheever AW, et al. Differential regulation of nitric oxide synthase-2 and arginase-1 by type 1/type 2 cytokines in vivo: granulomatous pathology is shaped by the pattern of L-arginine metabolism. J Immunol. 2001; 167:6533–44. [PubMed: 11714822]

[29]. Doyle AG, Herbein G, Montaner LJ, Minty AJ, Caput D, Ferrara P, et al. Interleukin-13 alters the activation state of murine macrophages in vitro: comparison with interleukin-4 and interferon-gamma. Eur J Immunol. 1994; 24:1441–5. [PubMed: 7911424]

[30]. Badylak SF, Valentin JE, Ravindra AK, McCabe GP, Stewart-Akers AM. Macrophage phenotype as a determinant of biologic scaffold remodeling. Tissue Eng Part A. 2008; 14:1835–42. [PubMed: 18950271]

[31]. Brown BN, Londono R, Tottey S, Zhang L, Kukla KA, Wolf MT, et al. Macrophage phenotype as a predictor of constructive remodeling following the implantation of biologically derived surgical mesh materials. Acta Biomater. 2012; 8:978–87. [PubMed: 22166681]

[32]. Zhou J, Tsai YT, Weng H, Tang L. Noninvasive assessment of localized inflammatory responses. Free Radic Biol Med. 2012; 52:218–26. [PubMed: 22080048]

[33]. Thevenot PT, Baker DW, Weng H, Sun MW, Tang L. The pivotal role of fibrocytes and mast cells in mediating fibrotic reactions to biomaterials. Biomaterials. 2011; 32:8394–403. [PubMed: 21864899]

[34]. Wang H, Zhao P, Liang X, Gong X, Song T, Niu R, et al. Folate-PEG coated cationic modified chitosan--cholesterol liposomes for tumor-targeted drug delivery. Biomaterials. 2010; 31:4129–38. [PubMed: 20163853]

[35]. Sun C, Sze R, Zhang M. Folic acid-PEG conjugated superparamagnetic nanoparticles for targeted cellular uptake and detection by MRI. J Biomed Mater Res A. 2006; 78:550–7. [PubMed: 16736484]

[36]. Nahar M, Jain NK. Preparation, characterization and evaluation of targeting potential of amphotericin B-loaded engineered PLGA nanoparticles. Pharm Res. 2009; 26:2588–98. [PubMed: 19842021]

[37]. Benoit M, Desnues B, Mege JL. Macrophage polarization in bacterial infections. Journal of Immunology. 2008; 181:3733–9.

[38]. Mills CD, Kincaid K, Alt JM, Heilman MJ, Hill AM. M-1/M-2 macrophages and the Th1/Th2 paradigm. J Immunol. 2000; 164:6166–73. [PubMed: 10843666]

[39]. Liew FY, Li Y, Moss D, Parkinson C, Rogers MV, Moncada S. Resistance to Leishmania major infection correlates with the induction of nitric oxide synthase in murine macrophages. Eur J Immunol. 1991; 21:3009–14. [PubMed: 1721024]

[40]. Jiang WW, Su SH, Eberhart RC, Tang L. Phagocyte responses to degradable polymers. J Biomed Mater Res A. 2007; 82:492–7. [PubMed: 17295256]

[41]. Weng H, Zhou J, Tang L, Hu Z. Tissue responses to thermally-responsive hydrogel nanoparticles. J Biomater Sci Polym Ed. 2004; 15:1167–80. [PubMed: 15503633]

[42]. Paulos CM, Turk MJ, Breur GJ, Low PS. Folate receptor-mediated targeting of therapeutic and imaging agents to activated macrophages in rheumatoid arthritis. Adv Drug Deliv Rev. 2004; 56:1205–17. [PubMed: 15094216]

[43]. Lu Y, Stinnette TW, Westrick E, Klein PJ, Gehrke MA, Cross VA, et al. Treatment of experimental adjuvant arthritis with a novel folate receptor-targeted folic acid-aminopterin conjugate. Arthritis Res Ther. 2011; 13:R56. [PubMed: 21463515]

[44]. Turk MJ, Waters DJ, Low PS. Folate-conjugated liposomes preferentially target macrophages associated with ovarian carcinoma. Cancer Lett. 2004; 213:165–72. [PubMed: 15327831]

[45]. Basu MK, Lala S. Macrophage specific drug delivery in experimental leishmaniasis. Curr Mol Med. 2004; 4:681–9. [PubMed: 15357216]

[46]. Barratt GM, Nolibe D, Yapo A, Petit JF, Tenu JP. Use of mannosylated liposomes for in vivo targeting of a macrophage activator and control of artificial pulmonary metastases. Ann Inst Pasteur Immunol. 1987; 138:437–50.

[47]. Muller CD, Schuber F. Neo-mannosylated liposomes: synthesis and interaction with mouse Kupffer cells and resident peritoneal macrophages. Biochim Biophys Acta. 1989; 986:97–105. [PubMed: 2819100]

[48]. Kassab R, Parrot-Lopez H, Fessi H, Menaucourt J, Bonaly R, Coulon J. Molecular recognition by Kluyveromyces of amphotericin B-loaded, galactose-tagged, poly (lactic acid) microspheres. Bioorg Med Chem. 2002; 10:1767–75. [PubMed: 11937335]

[49]. Puig-Kroger A, Sierra-Filardi E, Dominguez-Soto A, Samaniego R, Corcuera MT, Gomez-Aguado F, et al. Folate receptor beta is expressed by tumor-associated macrophages and constitutes a marker for M2 anti-inflammatory/regulatory macrophages. Cancer Res. 2009; 69:9395–403. [PubMed: 19951991]

[50]. Mukherjee S, Chen LY, Papadimos TJ, Huang S, Zuraw BL, Pan ZK. Lipopolysaccharide-driven Th2 cytokine production in macrophages is regulated by both MyD88 and TRAM. J Biol Chem. 2009; 284:29391–8. [PubMed: 19638630]

[51]. Hattori Y, Sakaguchi M, Maitani Y. Folate-linked lipid-based nanoparticles deliver a NFkappaB decoy into activated murine macrophage-like RAW264.7 cells. Biol Pharm Bull. 2006; 29:1516–20. [PubMed: 16819203]

[52]. Locke LW, Mayo MW, Yoo AD, Williams MB, Berr SS. PET imaging of tumor associated macrophages using mannose coated 64Cu liposomes. Biomaterials. 2012; 33:7785–93. [PubMed: 22840225]

[53]. Schierholz JM, Beuth J. Implant infections: a haven for opportunistic bacteria. J Hosp Infect. 2001; 49:87–93. [PubMed: 11567552]

[54]. Anderson JM. Mechanisms of Inflammation and Infection with Implanted Devices. Cardiovasc Pathol. 1993; 2:S33–S41.

[55]. Chen WT, Mahmood U, Weissleder R, Tung CH. Arthritis imaging using a near-infrared fluorescence folate-targeted probe. Arthritis Res Ther. 2005; 7:R310–7. [PubMed: 15743478]

[56]. Ruan G, Feng SS. Preparation and characterization of poly(lactic acid)-poly(ethylene glycol)-poly(lactic acid) (PLA-PEG-PLA) microspheres for controlled release of paclitaxel. Biomaterials. 2003; 24:5037–44. [PubMed: 14559017]

[57]. Koning GA, Schiffelers RM, Wauben MH, Kok RJ, Mastrobattista E, Molema G, et al. Targeting of angiogenic endothelial cells at sites of inflammation by dexamethasone phosphate-containing RGD peptide liposomes inhibits experimental arthritis. Arthritis Rheum. 2006; 54:1198–208. [PubMed: 16575845]

[58]. Nau GJ, Richmond JF, Schlesinger A, Jennings EG, Lander ES, Young RA. Human macrophage activation programs induced by bacterial pathogens. Proc Natl Acad Sci U S A. 2002; 99:1503–8. [PubMed: 11805289]

[59]. Michaelis M, Matousek J, Vogel JU, Slavik T, Langer K, Cinatl J, et al. Bovine seminal ribonuclease attached to nanoparticles made of polylactic acid kills leukemia and lymphoma cell lines in vitro. Anti-Cancer Drug. 2000; 11:369–76.

[60]. Drury JL, Mooney DJ. Hydrogels for tissue engineering: scaffold design variables and applications. Biomaterials. 2003; 24:4337–51. [PubMed: 12922147]

[61]. Nair A, Shen J, Lotfi P, Ko CY, Zhang CC, Tang L. Biomaterial implants mediate autologous stem cell recruitment in mice. Acta Biomater. 2011; 7:3887–95. [PubMed: 21784181]

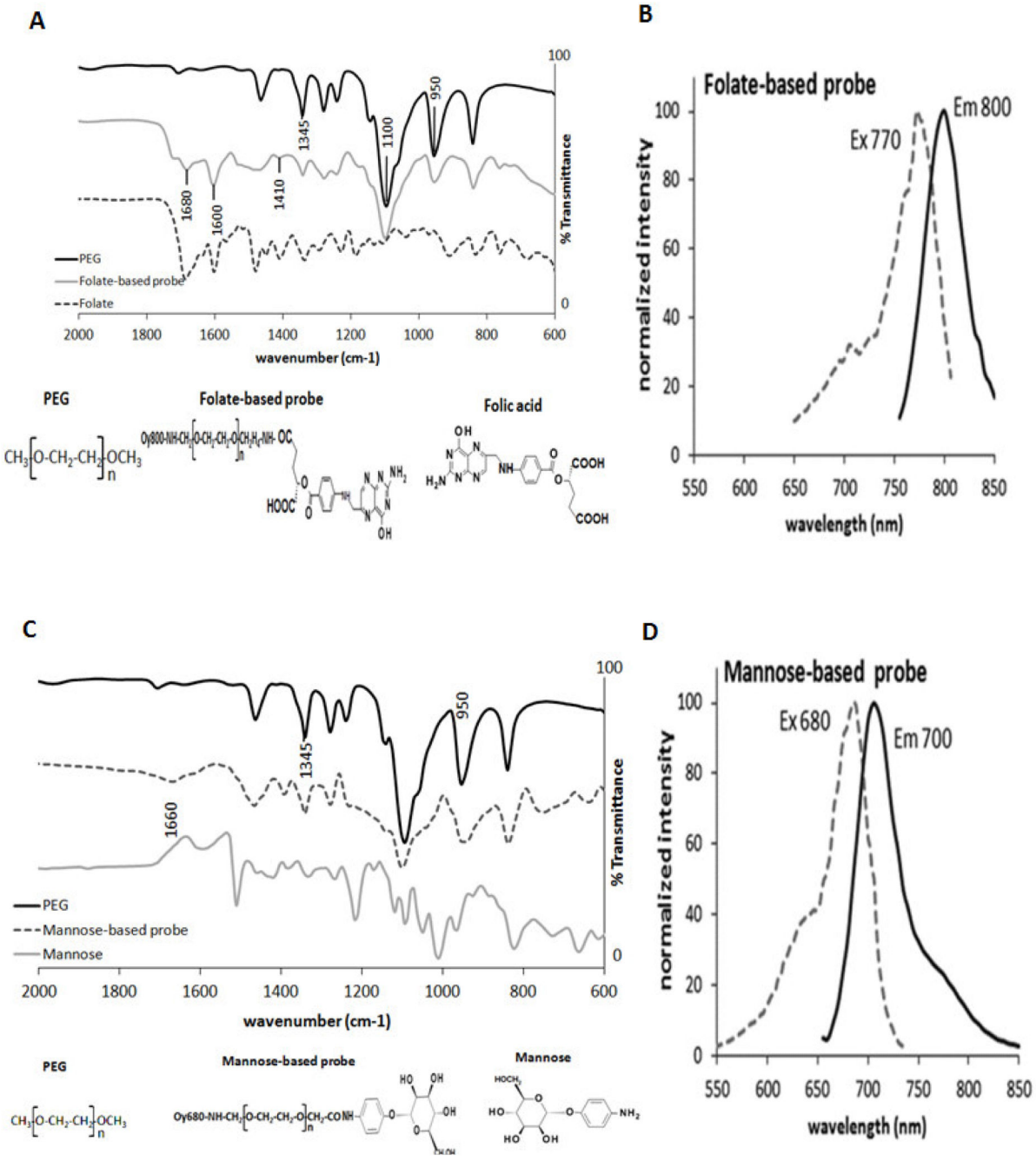

Figure 1.

Characterization of probes. (A) FTIR spectral characterization of PEG, folate-based probe, and folate. Characteristic PEG peaks are found at 1100 and 1345 cm^{-1} corresponding to the C-O-C stretch, and at 950cm^{-1} for the C-H bending. Conjugation of PEG and folate is confirmed by characteristic peaks at 1680 cm^{-1}, (amide link), and 1600, 1410 cm^{-1} (benzene ring of folate). (B) Histogram of excitation/ emission wavelengths of the folate-based probe shows maximal excitation and emission at 770 and 800nm respectively. (C) FTIR spectral characterization of PEG, mannose-based probe, and mannose. The appearance

of peaks at 1660cm^{-1} and 1390cm^{-1} demonstrate the conjugation of mannose to PEG by the presence of C=N stretch and of the amide bond respectively. (D) Histogram of excitation/emission wavelengths of the mannose-based probe shows maximal excitation and emission at 680 and 700nm respectively. The histograms (B&D) were normalized by adjusting the highest peaks to “100”.

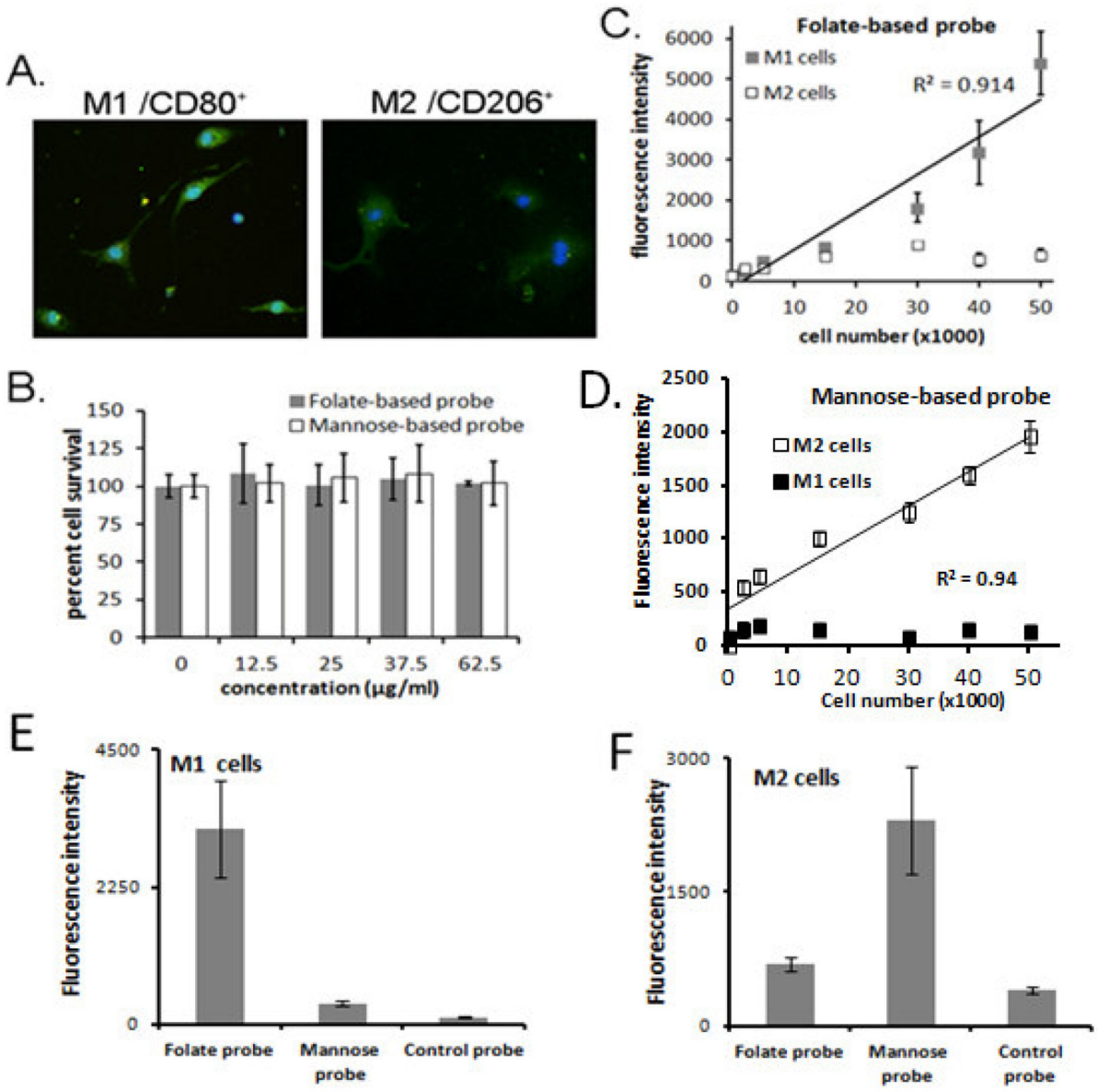

Figure 2.

In vitro studies. (A) Fluorescent images of M1 CD80$^+$ cells and M2 CD206$^+$ cells in culture. CD80$^+$ antibody and CD206$^+$antibody were used to stain M1 and M2 cells, respectively. (B) Toxicity results to 3T3 fibroblasts (up to 62.5 µg/ml) show no statistical differences from control (0 µg/ml probe) (6 replicates were run at each concentration). *In vitro* characterization of (C) folate-based probe specificity for M1 cells and (D) mannose-based probe specificity for M2 cells. Linear correlations are observed for the folate-based probe and M1 cells (R^2=0.914) and the mannose-based probe and M2 cells (R^2=0.94). Results are presented as the mean± standard deviation of 3 replicate experiments. (E) in vitro study to assess affinity of folate-based probe, mannose-based-probe and control probe to M1 cells. (F) in vitro study to assess affinity of mannose-based probe, folate-based probe and control probe to M2 cells.

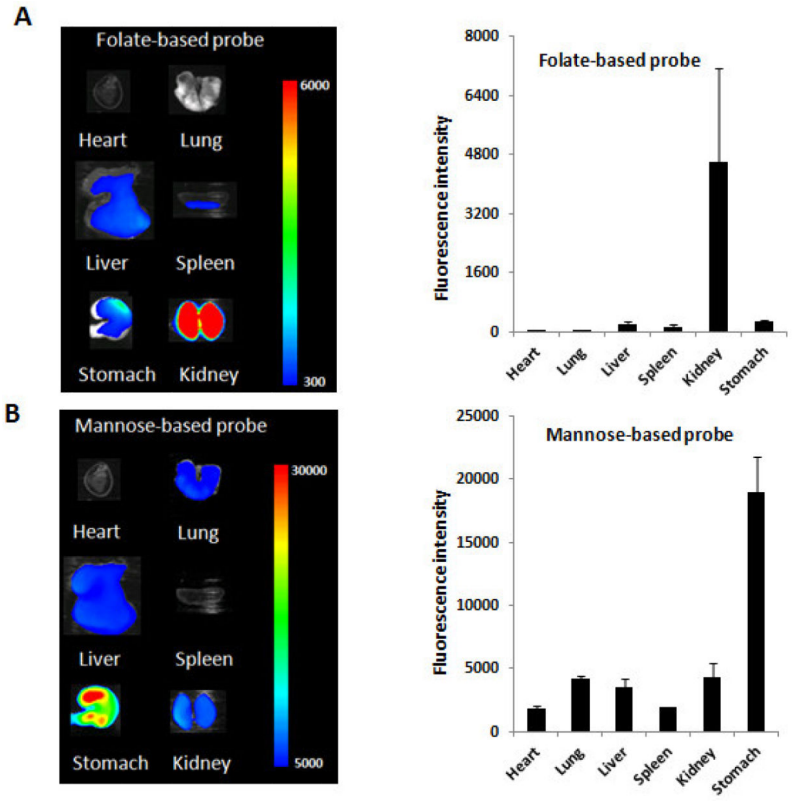

Figure 3.

(A) Ex vivo image and the mean fluorescence intensity (right) of mouse organs for the folate-based probe. (B) Ex vivo image and the mean fluorescence intensity (right) of mouse organs for the mannose-based probe.

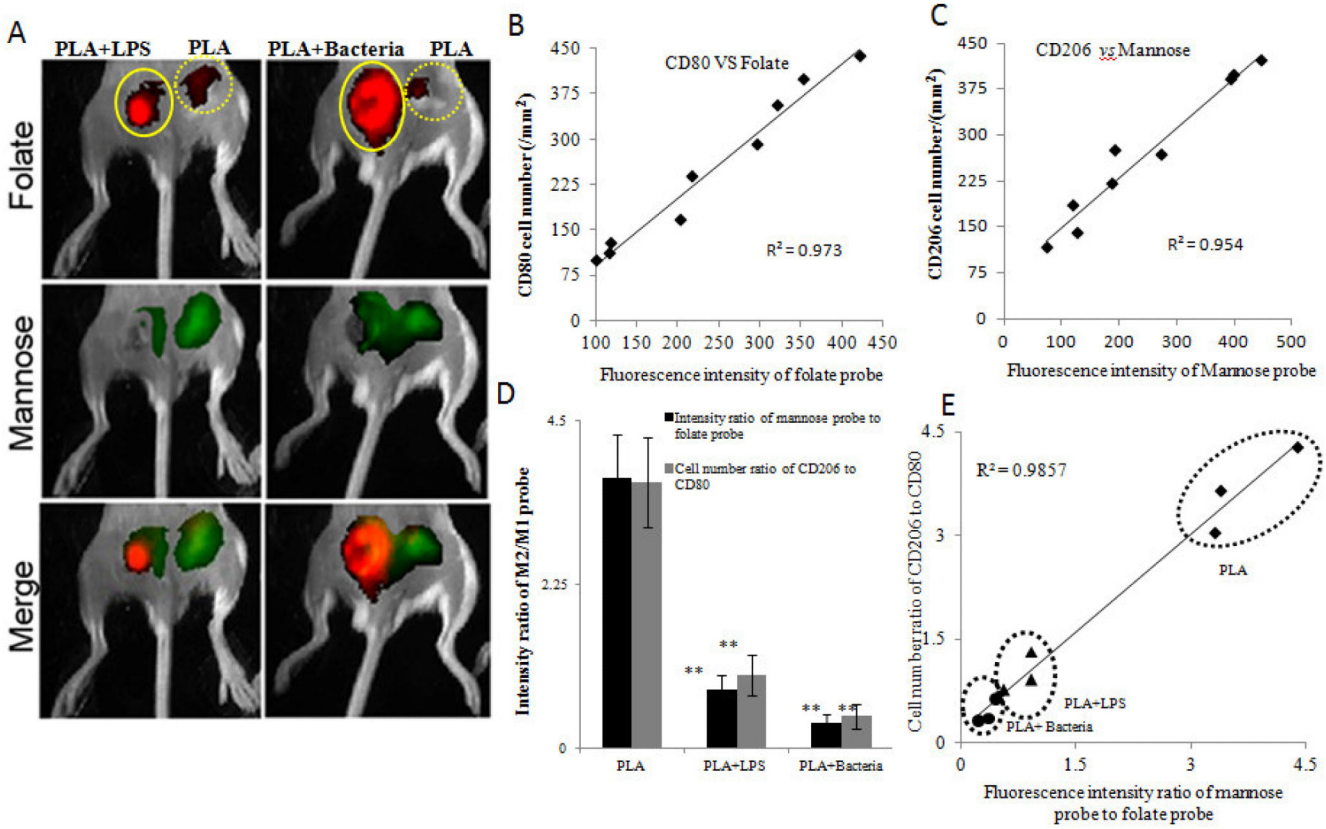

Figure 4.

Infection model. (A) *In vivo* imaging analysis of infection models comparing PLA particle implants to PLA+ LPS (labelled as +LPS) and PLA+ Bacteria (labelled as +Bacteria). In the panel, for each image, controls are on the right while +LPS or +Bacteria implants are on the left. Images are taken 48 hours after implantation. (B) Correlation between fluorescence intensity of the folate-based (M1) probe and CD80 cell density. (C) Correlation between fluorescence intensity of the mannose-based (M2) probe and CD206 cell density. (D) The M2/M1 ratios of the fluorescence intensity or the cellular numbers are comparatively similar showing a decreased ratio for both the +LPS and +Bacteria samples from the controls. (E) A positive correlation was found for the average cellular density ratio of M1 to M2 cells and the average fluorescent intensity ratio (M2/M1) as measured by the folate- and mannose-based probes for each sample implant (R^2=0.916). The experiment was run using n=3 mice with PLA and +LPS samples and then repeated with an additional n=3 mice using PLA and +Bacteria samples. In all histograms, statistical comparisons were made to the corresponding PLA control implant. Statistics were performed using one way ANOVA with Bonferroni correction. Error bar represents standard deviation (s.d.) and are considered significant when $P<0.05$(*) or $P < 0.01$(**).

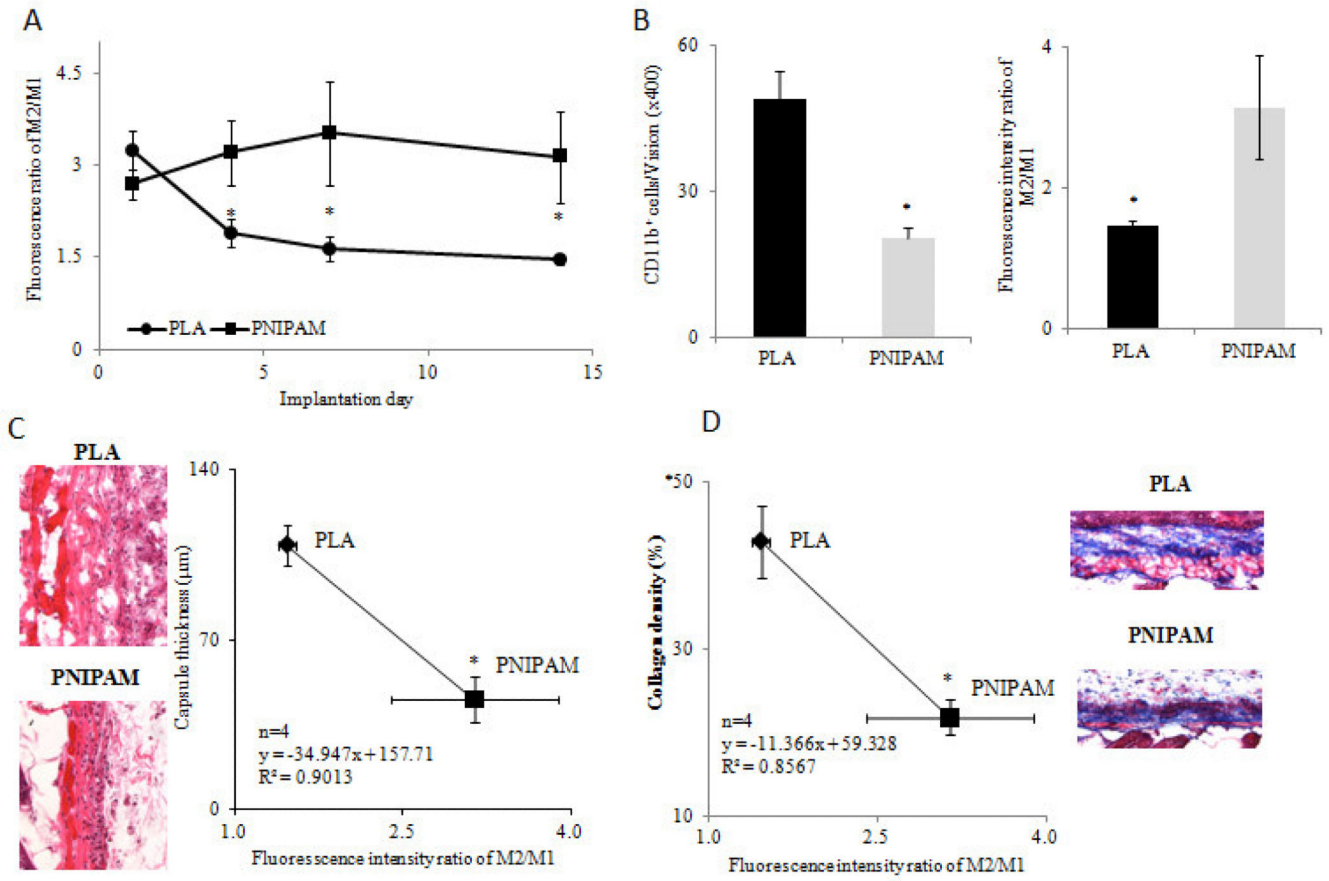

Figure 5.

Biomaterial model. (A) The fluorescence intensity ratio of M2/M1 with increasing implantation time. (B) Quantitative analysis of $CD11b^+$ cell density (left) and the fluorescence intensity ratios of M2/M1 (right) around 14-day implantation sites. (C) Representative images of H&E stained tissue sections (left) and linear relationship between the fluorescence intensity ratios of M2/M1 and the capsule thicknesses (right) at the 14-day particle implant sites. (D) Representative images of collagen stained tissue sections and linear relationship between the fluorescence intensity ratios of M2/M1 and the collagen densities at the 14-day particle implant sites. In the experiment, PLA and PNIPAM particles were implanted subcutaneously on the back of mice. 1, 4, 7 and 14 days after particle implantation, the folate- and mannose-based probe was injected intravenously. *In vivo* imaging was taken 48 hours after probe injection. At day 14, mice were imaged and implant surrounding tissue were then harvested for histological analysis. N=4 in all cases. Statistics were performed using Student's t-test between paired groups. Error bar represents standard deviation (s.d.) and are considered significant at $P<0.05$(*).